The reversible condensation and expansion of the rotavirus genome

Joseph B. Pesavento*†, Jeffrey A. Lawton*‡, Mary K. Estes§, and B. V. Venkataram Prasad*†¶

*Verna and Marrs McLean Department of Biochemistry and Molecular Biology, †W. M. Keck Center for Computational Biology, and §Department of Molecular Virology and Microbiology, Baylor College of Medicine, Houston, TX 77030

Edited by Wolfgang K. Joklik, Duke University Medical Center, Durham, NC, and approved November 29, 2000 (received for review September 14, 2000)

Understanding the structural organization of the genome is particularly relevant in segmented double-stranded RNA viruses, which exhibit endogenous transcription activity. These viruses are molecular machines capable of repeated cycles of transcription within the intact capsid. Rotavirus, a major cause of infantile gastroenteritis, is a prototypical segmented double-stranded RNA virus. From our three-dimensional structural analyses of rotavirus examined under various chemical conditions using electron cryomicroscopy, we show here that the viral genome exhibits a remarkable conformational flexibility by reversibly changing its packaging density. In the presence of ammonium ions at high pH, the genome condenses to a radius of ≈180 Å from ≈220 Å. Upon returning to physiological conditions, the genome re-expands and fully maintains its transcriptional properties. These studies provide further insights into the genome organization and suggest that the observed isometric and concentric nature of the condensation is due to strong interactions between the genome core and the transcription enzymes anchored to the capsid inner surface. The ability of the genome to condense beyond what is normally observed in the native virus indicates that the negative charges on the RNA in the native state may be only partially neutralized. Partial neutralization may be required to maintain appropriate interstrand spacing for templates to move around the enzyme complexes during transcription. Genome condensation was not observed either with increased cation concentrations at normal pH or at high pH without ammonium ions. This finding indicates that the observed genome condensation is a synergistic effect of hydroxyl and ammonium ions involving disruption of protein–RNA interactions that perhaps facilitate further charge neutralization and consequent reduction in the interstrand spacing.

double-stranded RNA virus | genome organization | electron cryomicroscopy

Endogenous transcription is a common and key molecular process that initiates gene expression in segmented double-stranded RNA (dsRNA) viruses (1–3). In these viruses, the genome is transcribed within an intact core, which contains the enzymatic machinery necessary for transcription. The resulting mRNA molecules are translocated through channels in the capsid layers (4, 5). Biochemical and structural studies on representative viruses such as orthoreovirus, cypovirus, and rotavirus indicate that genomic segments are transcribed independently and simultaneously (4–6). The transcriptionally active particles of these viruses are capable of repeated cycles of transcription. Structural studies on several dsRNA viruses indicate that the transcription enzymes are anchored to the inner surface of the capsid surrounded by the genome, thereby suggesting that the RNA template moves around these enzymes (7–11). During the process of transcription, the template must be unwound, separated, transcribed, rejoined, and rewound for further cycles of transcription. All of these data suggest that genome transcription in dsRNA viruses is a highly dynamic process.

Central to our understanding of the molecular process of endogenous transcription in these viruses is knowledge of the structural organization of their genomes. Although structural studies have provided a wealth of information on the capsid architecture in some of the dsRNA viruses, several questions still remain regarding the genome and the nature of chemical interactions that can facilitate such an orchestrated movement of the dsRNA around the enzyme complex. Recent x-ray crystallographic structures of transcriptionally competent cores of bluetongue virus and orthoreovirus have provided an unprecedented look at the capsid organization at the atomic level (12, 13) and shown that a significant amount of the genome is statistically ordered and manifest as concentric shells of density spaced at 26–30 Å.

The focus of our study, rotavirus, belongs to the *Reoviridae* family. Its genome consists of 11 dsRNA segments, each coding for at least one viral protein, of which six are structural and six are nonstructural proteins (14). Earlier structural studies have shown that the genome is packaged within a capsid consisting of three concentric icosahedrally organized protein layers (15). The innermost layer, in the immediate vicinity of the genome, is made of VP2, which is known to be an RNA binding protein (16, 17). A significant portion of the dsRNA, which is in close contact with the VP2 layer, is icosahedrally ordered (7). The two enzymes responsible for endogenous transcription, VP1, the RNA-dependent RNA polymerase (18), and VP3, the guanylyl and methyl transferase (19, 20), are attached as a complex to the inside surface of the VP2 layer at all of the 5-fold positions (7). The middle layer with $T = 13$ icosahedral symmetry is composed of VP6, and the outer layer exhibiting the same icosahedral symmetry is composed of the glycoprotein VP7 and the spike protein VP4 (7, 21, 22). VP4 has been implicated in cell attachment and entry, neutralization, hemagglutination, and virulence (14). During cell entry, the mature triple-layered particle (TLP) loses its outer layer and the resulting double-layered particle (DLP) becomes transcriptionally active. Structural studies on the actively transcribing DLPs have shown that the newly synthesized mRNA molecules exit through the channels at the 5-fold vertices (5).

To gain a greater understanding into the organization of the genome in rotavirus, we have taken the approach of perturbing the structure by varying chemical conditions such as pH and ionic strength. The underlying assumption is that the protein–RNA interactions and charged nature of the RNA are critical factors in determining the structural organization of the genome inside the virions. Unlike the capsid portion, the genomic portion

This paper was submitted directly (Track II) to the PNAS office.

Abbreviations: dsRNA, double-stranded RNA; TLP, triple-layered particle; DLP, double-layered particle.

‡Present address: Department of Chemistry and Biochemistry, University of California, San Diego, CA 92093.

¶To whom reprint requests should be addressed. E-mail: vprasad@bcm.tmc.edu.

The publication costs of this article were defrayed in part by page charge payment. This article must therefore be hereby marked "*advertisement*" in accordance with 18 U.S.C. §1734 solely to indicate this fact.

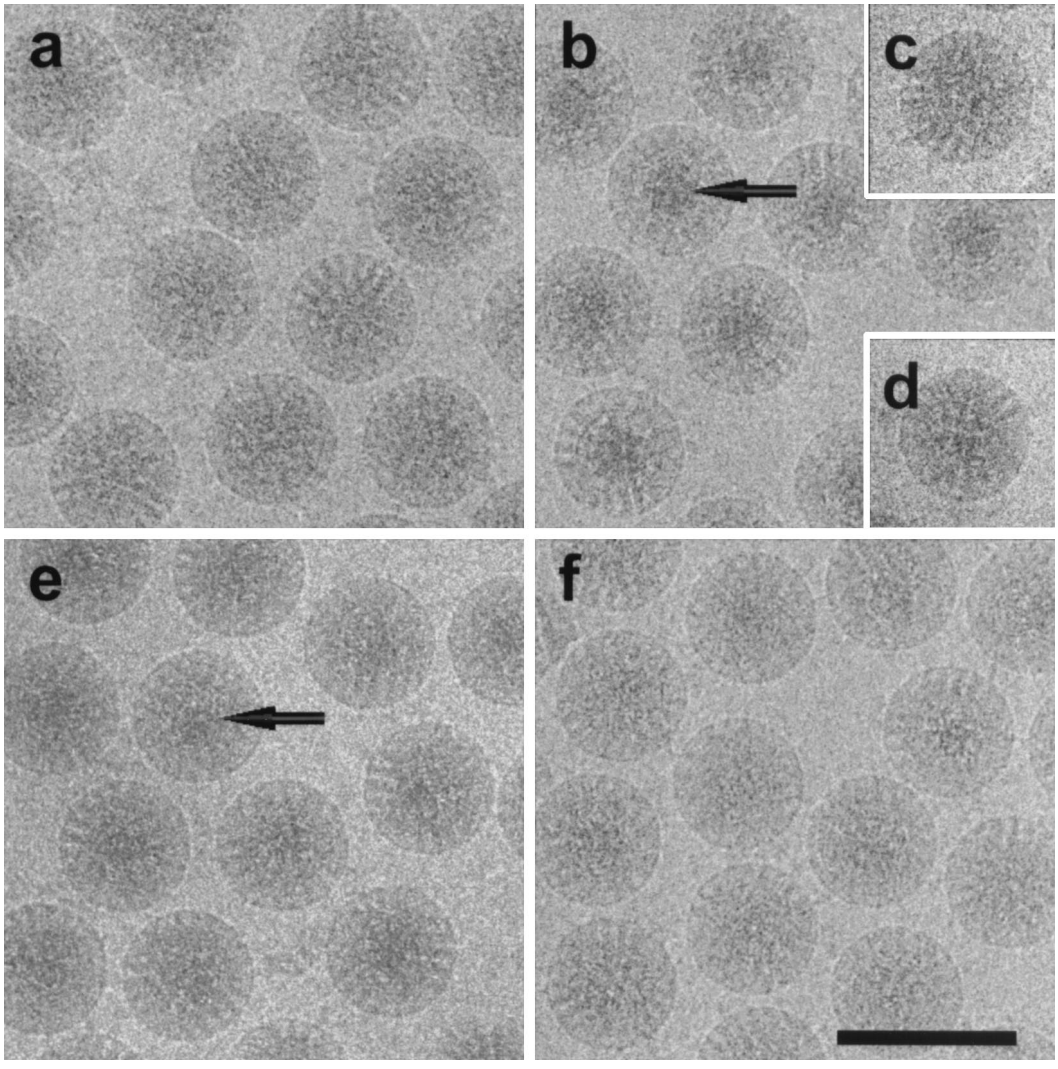

Fig. 1. Electron cryomicrograph of rotavirus SA11–4F TLPs embedded in vitreous ice under various chemical conditions. (*a*) TNC (10 mM Tris, 150 mM NaCl, 10 mM $CaCl_2$, pH 7.5). (*b*) 250 mM NH_4OH (pH 11.5); arrow indicates condensed RNA in the center of each particle. (*c*) 3-[cyclohexylamino]-1-propanesulfonic acid) (CAPS) buffer, pH 11.6. (*d*) 250 mM NH_4Cl in TNC (pH 7.5). (*e*) TNC (pH 9.0) after NH_4OH treatment (pH 11.5). (*f*) TNC (pH 7.5) after NH_4OH treatment (pH 11.5). (Scale bar: 1,000 Å.)

of the virion is not directly amenable to three-dimensional structural analysis because of the icosahedral averaging that is implicitly used in the structure determination of icosahedral viruses either by x-ray crystallography or electron cryomicroscopy techniques. Although not strictly icosahedral, the appearance of the genome density in the icosahedrally averaged structure as concentric layers provides a tractable signature to examine the effect of various conditions on the genome organization. From our three-dimensional structural analyses of rotavirus under various chemical conditions using electron cryomicroscopy, which is ideally suited for such analyses, we have made several interesting observations that have direct implications on the structural organization of the genome.

Materials and Methods

Cells and Virus. Rotavirus TLPs (SA11–4F strain) grown in the presence of trypsin in MA-104 simian cells, were purified as described and suspended in TNC buffer (10 mM Tris/150 mM NaCl/10 mM $CaCl_2$, pH 7.5) (21). To study the effect of various chemical conditions on the virus, the specimen was dialyzed by using a microdialysis button (Hampton Research, Riverside, CA) for 30 min in the appropriate solutions as specified in *Results*.

Electron Cryomicroscopy. Specimen preparation for cryomicroscopy was carried out by using standard procedures (23). Electron micrographs were recorded on a JEOL 1200 transmission electron microscope operating at 100 kV with a magnification of $\times$30,000 using an electron dose of 5 $e^-/Å^2$. From each specimen area in the grid, a focal pair with intended defocus values of 1 and 2 μm was recorded.

Three-Dimensional Reconstructions. Micrographs were selected for correct defocus, ice quality, contrast, and particle concentration and were digitized by using a Zeiss SCAI microdensitometer with a scanning interval of 14 μm corresponding to 4.67 Å in the object. Determination of the defocus values (24), orientation determination and refinement (25, 26), three-dimensional reconstruction, resolution assessment (27), and corrections for contrast-transfer-function (CTF) were carried out as described (7, 28). Reconstructions were carried out by using the data from closer-to-focus images to a resolution within the first zero of the CTF with appropriate corrections using the defocus values of

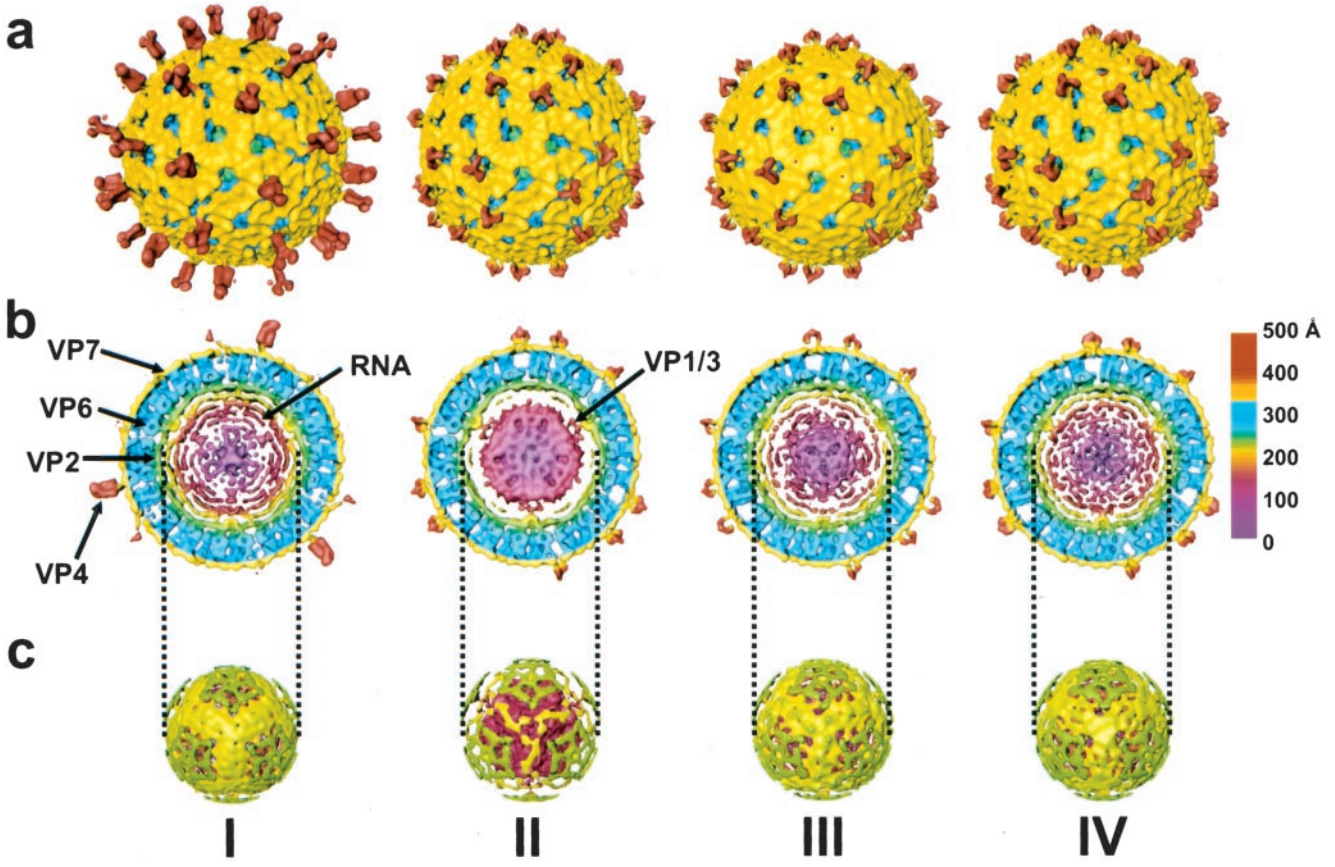

Fig. 2. Three-dimensional reconstructions of rotavirus under various chemical conditions. (*I*) TNC (pH 7.5). Arrows indicate various structural proteins and RNA. (*II*) 250 mM NH_4OH (pH 11.5). Arrow indicates interaction between condensed RNA and VP1/VP3 complex. (*III*) TNC (pH 9.0) after NH_4OH (pH 11.5). (*IV*) TNC (pH 7.5) after NH_4OH (pH 11.5). The reconstruction is radially colored from the center to indicate the various protein layers according to the chart at the right. (*a*) Surface representations of the TLPs looking down the icosahedral 3-fold axis. The VP4 protein is red and VP7 is yellow. (*b*) Equatorial slice (≈47 Å thick) from the reconstruction. The VP6 protein is blue, VP2 is green, and the VP1/VP3 complex is red. The inner RNA layers are shown in colors ranging from yellow to maroon. (*c*) Surface representation at a radius of ≈233 Å showing the outer layer of RNA in yellow and the remnants of VP2 in green.

−1.4 μm (pH 7.5), −1.4 μm (pH 11.5), −1.5 (pH 9.0 from 11.5), and −1.4 (pH 7.5 from 11.5). The reconstructions and the radial density profiles remained essentially the same before and after the CTF corrections. For each reconstruction, the number of particles with unique orientations was found to be adequate by examining the spread of inverse eigen values, which was less than 0.1 for 99% of the data. After the final refinement, in each case, the average phase residual between the images and their corresponding projections was less than 45°. Threshold values for the reconstructions were chosen to account for 780 molecules of VP6 between a radius of 250 and 350 Å in all reconstructions.

Transcription Assays. Ten micrograms of DLPs was dialyzed against 250 mM NH_4OH (pH 11.5) for 25 min, back to pH 7.5 with TNC, then finally to PBS, pH 7.5 (to remove Ca^{2+} from the TNC). Both native and pH-treated DLPs were suspended in 20 μl of a transcription reaction buffer and radiolabeled and electrophoresed as described (29). To quantitate transcript yields and rates, transcription reactions were set up under equivalent conditions using [5, 6-^{3}H]UTP (44 Ci/mmol, Amersham Pharmacia) to radiolabel the transcripts. Aliquots were removed at the times indicated, dried onto glass fiber filters, and washed twice with 5% trichloroacetic acid and once with 70% ethanol. Radioactivity incorporated into trichloroacetic acid insoluble material was determined by liquid scintillation counting.

Results

RNA Condenses at Ammonium High pH. As a control and reference, the structure of the rotavirus at normal physiological conditions (pH 7.5) was determined. The electron cryomicrograph (Fig. 1*a*) and the corresponding reconstruction (Fig. 2*I*) from 322 particles of native rotavirus computed to a resolution of ≈23 Å show all of the structural features described by earlier studies. The surface representation of the structure (Fig. 2*aI*) shows the external features such as the VP4 spikes and the VP7 layer with channels at the 5- and 6-coordinated positions of the $T = 13$ icosahedral lattice. The internal features are shown in the equatorial cross-sectional slice (Fig. 2*bI*). The concentric layers of genomic RNA can be seen in the center within the VP2 layer (in green) surrounding the VP1/VP3 complexes which are attached to the inner surface of VP2 layer at the icosahedral 5-fold vertices. These layers of RNA, which appear as peaks in the radial density profile (Fig. 3*a*), start at a radius of ≈220 Å and are spaced on average about 28 Å apart. A surface representation of the virion structure at a radius of ≈233 Å shows the icosahedrally ordered portion of the RNA in yellow (Fig. 2*cI*).

In contrast to particle images at normal physiological conditions (Fig. 1*a*), cryo-images of particles under ammonium high pH conditions (250 mM NH_4OH, pH 11.5) show a distinct high-density feature at the center of each particle (Fig. 1*b*). In this condition, the reconstruction (Fig. 2*II*) using 246 particles computed to a resolution of ≈23 Å indicates two major structural changes with respect to the native structure. First, the spike

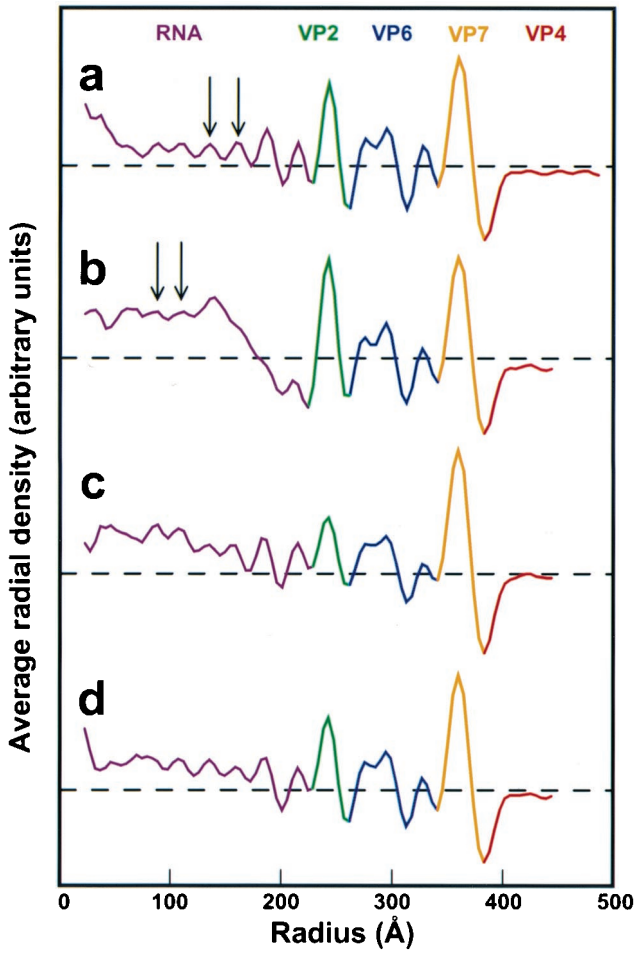

Fig. 3. Radial density plots computed from the reconstructions after contrast-transfer-function correction. (*a*) TNC (pH 7.5). (*b*) 250 mM NH_4OH (pH 11.5). (*c*) TNC (pH 9.0) after NH_4OH (pH 11.5). (*d*) TNC (pH 7.5) after NH_4OH (pH 11.5). Arrows indicate peaks of average RNA density. The dashed horizontal line represents an averaged radial density of zero.

protein VP4 has undergone a dramatic conformational change. The long VP4 spike of length ≈105 Å seen in the native virion is altered to a short tri-lobed stub of ≈50 Å in length (Fig. 2*aII*). In contrast to the native spike that has two connections to the VP7 layer, the altered spike has three connections. The volume occupied by the altered spike clearly indicates that there is a significant loss of mass.

The second major structural change is in the genomic RNA. The viral genome is condensed to a mass of radius ≈180 Å as seen in the equatorial slice of the structure (Fig. 2*bII*). The condensed RNA core, although well separated from the VP2 capsid layer, is still in contact with the VP1/VP3 complexes. Such condensation is the reason for the observed dark features in the cryo-images (Fig. 1*b*). The radial density profile (Fig. 3*b*) shows that the RNA layers have shifted toward the center and appear to have a tighter spacing than at the native condition.

Structural Change in the Genome Is Reversible. To examine whether the observed RNA condensation is reversible, the virus was brought back to lower pH after ammonium high pH treatment. The cryo-images of the particles after lowering to pH 9 appeared more native-like with some slight electron dense regions still visible in the center (Fig. 1*e*). With this condition, the reconstruction using 117 particles to a resolution of ≈23 Å, revealed that the VP4 spike remains stunted (Fig. 2*aIII*), indicating that the conformational change in the spike is irreversible. However, the genome appeared to be in the process of regaining its native structure. Although there is still some condensed RNA near the center, the expanded RNA layers close to the VP2 layer are clearly apparent (Figs. 2*bIII* and 3*c*). To examine whether the native genome organization could be completely restored, the virus was brought back from ammonium high pH to pH 7.5. The cryo-images of the virions under this condition showed that the central dark feature is no longer present (Fig. 1*f*). The reconstruction using 149 particles to a resolution of ≈22 Å clearly shows that the genomic RNA is fully expanded and has native-like appearance (Fig. 2*bIV*). The radial density profile verifies that the peaks of RNA density have returned to a spacing of ≈28 Å (Fig. 3*d*).

Ammonium High pH-Treated Rotavirus Is Transcriptionally Competent. To examine whether the alterations in the genome organization had any lasting effect on the transcriptional ability of the virus, transcriptionally competent particles (DLPs) obtained by removing the outer layer from TLPs were dialyzed in ammonium high pH, brought back to the normal condition and analyzed by using a transcription assay. As visualized by high-resolution denaturing PAGE, the length distribution of mRNA transcripts was similar in both the native and pH-treated DLPs (Fig. 4*a*). In addition, both the rate of transcription (Fig. 4*b*) and the overall yield of mRNA after 30 min (Fig. 4*c*) were nearly equivalent in both kinds of particles. These results indicate that the condensation and re-expansion did not have any deleterious effect on the genomic RNA, and that upon re-expansion, the necessary interactions between the internal proteins (VP1, VP2, and VP3) and the genomic RNA were restored.

High pH Alone Cannot Cause Genome Condensation. To determine whether the RNA condensation was due to the presence of ammonium or hydroxide ions, or a combination of the two, we tested the virus separately under each condition. Cryo-images of virus dialyzed in CAPS (3-[cyclohexylamino]-1-propanesulfonic acid) buffer titrated to pH 11.6 by using NaOH shows no central dark features (Fig. 1*c*). The reconstruction confirmed that there was no RNA condensation (data not shown), but that the VP4 spike was stunted as in the ammonium high pH experiments. To see whether the RNA condensation was due solely to the cation NH_4^+, virus was dialyzed in a buffer with 250 mM NH_4Cl (pH 7.5). The micrographs showed no indication of RNA condensation (Fig. 1*d*). The reconstruction showed no structural alterations either with respect to VP4 or RNA. High concentrations of divalent cation (1 M $MgCl_2$) also failed to induce any condensation.

Discussion

One of the startling results of our studies is the condensation of the genomic RNA at ammonium high pH conditions. The observed reversible condensation and expansion without compromising the functional ability of RNA indicates that this process represents a structural transformation. The prevalent idea concerning the packaging of genomes into virus capsids is that counter ions like Mg^{2+}, or polyamines like spermine and spermidine, neutralize charges on the nucleic acid (30). In the case of rotavirus and other dsRNA viruses, the internal proteins (VP2, VP1, and VP3) also may contribute significantly toward charge neutralization. If the charge on the rotaviral genome is already neutralized, what is the cause for further condensation that we have observed here? One possibility is that rotaviral RNA is not completely neutralized in the native state. Disruption of some protein–RNA interactions together with some conformational changes in the RNA at high pH may facilitate complete charge neutralization and hence further condensation. A possible mechanism is that NH_4^+, perhaps by displacing water molecules, may bridge the adjacent strands by hydrogen bonding

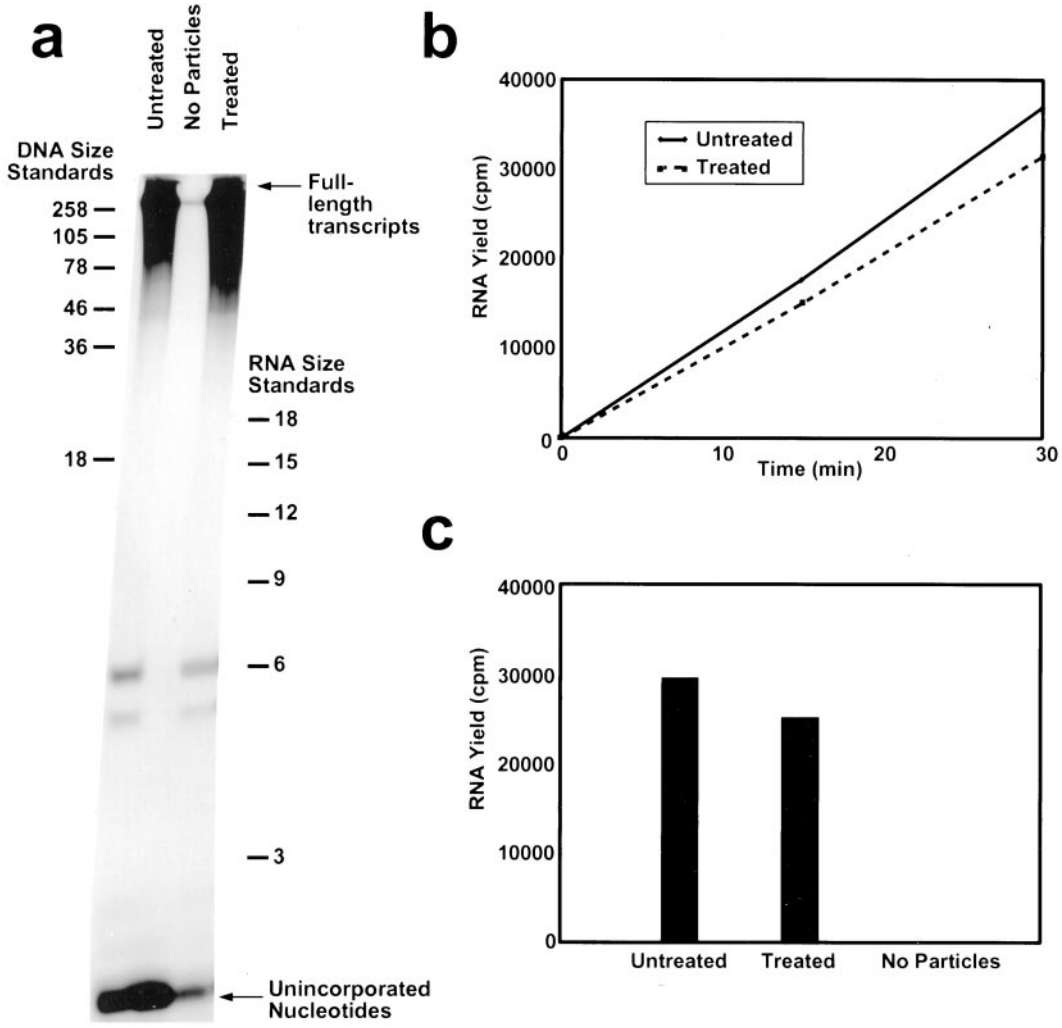

Fig. 4. Transcription assay of normal (pH 7.5) and ammonium high pH-treated DLPs. (*a*) High-resolution polyacrylamide gel (PAGE) analysis of transcription reaction mixtures containing native DLPs (Untreated) and DLPs brought back to native conditions after ammonium high pH treatment (Treated). The middle lane contained no particles. (*b*) RNA yield in transcription assay at 0, 15, and 30 min. (*c*) Quantitation of RNA yield after 30 min.

to their phosphate oxygens and reduce the interstrand spacing to cause condensation. Such hydrogen bond formation also may act as electrostatic shielding and reduce the repulsion between the strands. The NH_4^+ and OH^- may act synergistically in causing the condensation. The simple disruption of the protein–RNA interactions, as may happen in the case of high pH (OH^-), is not sufficient alone to induce condensation. The conformation of the RNA in the native state may not allow further charge neutralization, as in the experiments with increased NH_4^+ or Mg^{2+} cations at normal pH.

An important observation is that the condensation is concentric with respect to the particle center. It is clear from the micrographs as well as the reconstructions that the condensed RNA remains at the center of the particle. This would not have been the case if the condensed RNA were completely disassociated from the capsid inner surface. Although dissociated from the VP2 layer, the genome still maintains contacts with the symmetrically located VP1/VP3 complexes. In terms of the structural organization of the genome, this observation clearly indicates that interaction of the genome with the transcription enzymes is a critical factor and supports the notion that each dsRNA segment may be associated with a VP1/VP3 complex (7).

In addition to interaction with the VP1/VP3 complex, the interaction with VP2 is likely to be an important factor in the structural organization of the genome. Upon returning to normal conditions, the genome expands and restores all of the native contacts with the VP2 layer. VP2 is an RNA binding protein with an internally located basic N-terminal region (16, 17). Genome interactions with VP2 may be important for maintaining the appropriate spacing between the dsRNA strands in the native expanded state, and disruption of these interactions at high pH, possibly due to deprotonation of critical VP2 residues, may initiate the observed condensation. Assuming that dsRNA behaves like dsDNA (31, 32), at the concentration of ≈400 mg/ml in the native state [estimated from the molecular mass (≈10.0×10^6 Da) and the volume of the genome] the RNA strands are likely to exhibit local hexagonal packing with an interstrand spacing of 30–32 Å. Such spacing translates to 26- to 28-Å separation between the RNA layers typically observed in icosahedrally averaged structures of native rotavirus, bluetongue virus (12), and orthoreovirus (13). For the condensed state, with an estimated concentration of ≈680 mg/ml, the expected interstrand spacing is ≈25 Å. It is possible that the implied partial neutralization of RNA is necessary to keep the optimum distance of about ≈31 Å between the strands in the native state,

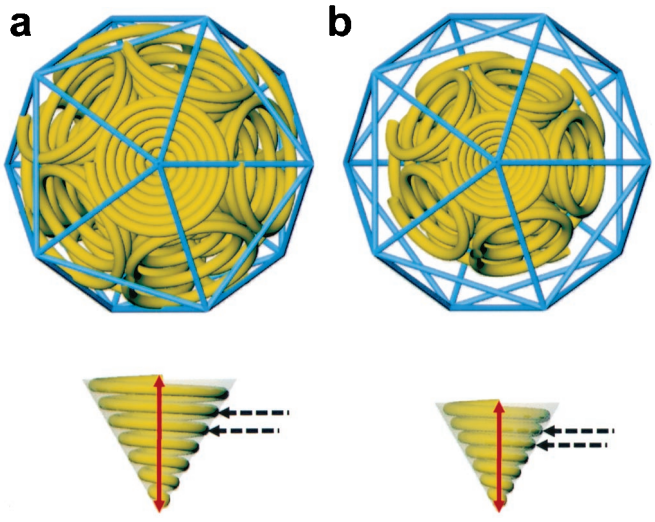

Fig. 5. Model of RNA packaging and condensation. (*a*) RNA organization under normal physiological conditions. Each yellow spiral represents a single dsRNA genome segment; the entire genome model is shown surrounded by an icosahedral lattice in blue. (*b*) Proposed RNA organization at ammonium high pH conditions. The red arrow represents the height, ≈220 Å in *a* and ≈180 Å in *b*, of a spiral cone. The dashed black arrows indicate the spacing, ≈31 Å in *a* and ≈25 Å in *b*, between the center of each dsRNA helix.

which may be conducive to allowing the RNA template to move around the transcription enzyme complex.

Any model for the structural organization of the genome in a segmented dsRNA virus, particularly in the *Reoviridae*, should allow for simultaneous and independent transcription of the segments as well as for repeated cycles of transcription. Our present studies impose on such a model another constraint of reversible condensation and expansion. Gouet *et al.* (33) have proposed a plausible model in which each segment is spooled around a transcriptase complex. This model allows for up to 12 independent transcription complexes, each with an individual dsRNA segment attached for concurrent transcription. A stylized version of this model, taking into consideration the diameter of the dsRNA as ≈20 Å, and the interstrand spacing of ≈31 Å in the expanded state of the genome, is shown in Fig. 5*a*. In this model, each dsRNA segment is depicted as an inverted cone at the 5-fold vertex surrounding a transcription enzyme complex. When the interstrand separation is reduced to ≈25 Å, the genome core collapses to the observed radius of ≈180 Å (Fig. 5*b*). This observation provides a simple mechanistic explanation for our observations and suggests that condensation is essentially a consequence of reduced interstrand spacing.

Our results demonstrate the remarkable stability of the capsid and resilience of the genome, which may be the required attributes to carry out continuous transcription of multiple genome segments within the confines of the capsid. The ability of the genome to reversibly condense and expand indicates that the dsRNA has a certain degree of flexibility and suggests that the packaged genome is not at its highest condensed state at normal physiological conditions. Ultimately, however, it may be the normal, expanded state that is most conducive for efficient transcription. The observed concentric condensation suggests that the transcription enzyme complex plays a major role in the structural organization of the genome and supports a model in which each complex is associated with a genome segment. The model presented here allows for the observed reversible condensation and expansion as well as the independent synthesis of genome transcripts with minimal interference from neighboring genome segment/transcription complexes.

We thank S. Mukherjee for electron microscopy assistance, M. Dougherty for computer graphics assistance, and T. Wensel for helpful discussions. This work was supported by National Institutes of Health Grants AI-36040 (B.V.V.P.) and DK-30144 (M.K.E.). J.B.P. acknowledges the support of National Science Foundation Training Grant BIR-9256580. We also gratefully acknowledge the use of facilities at the National Center of Macromolecular Imaging, supported by a grant from the National Institutes of Health (RR02250), and the Biomedical Computational and Visualization Laboratory, supported by a grant from the National Science Foundation.

1. Fields, B. N. (1996) in *Fields Virology*, ed. Fields, B. N. (Lippincott–Raven, Philadelphia), Vol. 2, pp. 1553–1555.
2. Joklik, W. K. (1983) in *The Reoviridae*, ed. Joklik, W. K. (Plenum, New York), pp. 1–7.
3. Mindich, L. (1999) *Microbiol. Mol. Biol. Rev.* **63,** 149–160.
4. Gillies, S., Bullivant, S. & Bellamy, A. R. (1971) *Science* **174,** 694–696.
5. Lawton, J. A., Estes, M. K. & Prasad, B. V. V. (1997) *Nat. Struct. Biol.* **4,** 118–121.
6. Smith, R. E. & Furuichi, Y. (1982) *J. Virol.* **41,** 326–329.
7. Prasad, B. V. V., Rothnagel, R., Zeng, C. Q., Jakana, J., Lawton, J. A., Chiu, W. & Estes, M. K. (1996) *Nature (London)* **382,** 471–473.
8. Dryden, K. A., Farsetta, D. L., Wang, G., Keegan, J. M., Fields, B. N., Baker, T. S. & Nibert, M. L. (1998) *Virology* **245,** 33–46.
9. Butcher, S. J., Dokland, T., Ojala, P. M., Bamford, D. H. & Fuller, S. D. (1997) *EMBO J.* **16,** 4477–4487.
10. Hill, C. L., Booth, T. F., Prasad, B. V. V., Grimes, J. M., Mertens, P. P., Sutton, G. C. & Stuart, D. I. (1999) *Nat. Struct. Biol* **6,** 565–568.
11. Nason, E. L., Samal, S. K. & Prasad, B. V. V. (2000) *J. Virol.* **74,** 6546–6555.
12. Grimes, J. M., Burroughs, J. N., Gouet, P., Diprose, J. M., Malby, R., Zientara, S., Mertens, P. P. & Stuart, D. I. (1998) *Nature (London)* **395,** 470–478.
13. Reinisch, K. M., Nibert, M. L. & Harrison, S. C. (2000) *Nature (London)* **404,** 960–967.
14. Estes, M. K. (1996) in *Fields Virology*, ed. Fields, B. N. (Lippincott–Raven, Philadelphia), Vol. 2, pp. 1625–1655.
15. Prasad, B. V. V. & Estes, M. K. (1997) in *Structural Biology of Viruses*, ed. Chiu, W. (Oxford Univ. Press, Oxford), pp. 239–268.
16. Labbe, M., Baudoux, P., Charpilienne, A., Poncet, D. & Cohen, J. (1994) *J. Gen. Virol.* **75,** 3423–3430.
17. Lawton, J. A., Zeng, C. Q., Mukherjee, S. K., Cohen, J., Estes, M. K. & Prasad, B. V. V. (1997) *J. Virol.* **71,** 7353–7360.
18. Valenzuela, S., Pizarro, J., Sandino, A. M., Vasquez, M., Fernandez, J., Hernandez, O., Patton, J. & Spencer, E. (1991) *J. Virol.* **65,** 3964–3967.
19. Liu, M., Mattion, N. M. & Estes, M. K. (1992) *Virology* **188,** 77–84.
20. Chen, D., Luongo, C. L., Nibert, M. L. & Patton, J. T. (1999) *Virology* **265,** 120–130.
21. Shaw, A. L., Rothnagel, R., Chen, D., Ramig, R. F., Chiu, W. & Prasad, B. V. V. (1993) *Cell* **74,** 693–701.
22. Yeager, M., Berriman, J. A., Baker, T. S. & Bellamy, A. R. (1994) *EMBO J.* **13,** 1011–1018.
23. Dubochet, J., Adrian, M., Chang, J. J., Homo, J. C., Lepault, J., McDowall, A. W. & Schultz, P. (1988) *Q. Rev. Biophys.* **21,** 129–228.
24. Zhou, Z. H., Prasad, B. V. V., Jakana, J., Rixon, F. J. & Chiu, W. (1994) *J. Mol. Biol.* **242,** 456–469.
25. Crowther, R. A. (1971) *Philos. Trans. R. Soc. London B* **261,** 221–230.
26. Fuller, S. D. (1987) *Cell* **48,** 923–934.
27. van Heel, M. (1987) *Ultramicroscopy* **21,** 95–100.
28. Lawton, J. A. & Prasad, B. V. V. (1996) *J. Struct. Biol.* **116,** 209–215.
29. Lawton, J. A., Estes, M. K. & Prasad, B. V. V. (1999) *Proc. Natl. Acad. Sci. USA* **96,** 5428–5433.
30. Bloomfield, V. A. (1997) *Biopolymers* **44,** 269–282.
31. Livolant, F. & Leforestier, A. (1996) *Prog. Polym. Sci.* **21,** 1115–1164.
32. Podgornik, R., Strey, H. H., Rau, D. C. & Parsegian, V. A. (1995) *Biophys. Chem.* **57,** 111–121.
33. Gouet, P., Diprose, J. M., Grimes, J. M., Malby, R., Burroughs, J. N., Zientara, S., Stuart, D. I. & Mertens, P. P. (1999) *Cell* **97,** 481–490.